RSC Advances

ROYAL SOCIETY OF CHEMISTRY

www.rsc.org/advances

Graphical Abstract

Efficient visible light photodegradation of Methylene blue using TiO_2- graphene based composites has been reported. DFT calculations corroborate the mechanism for Ti-O-C bond formation, leading to an additional band edge and band gap tuning.

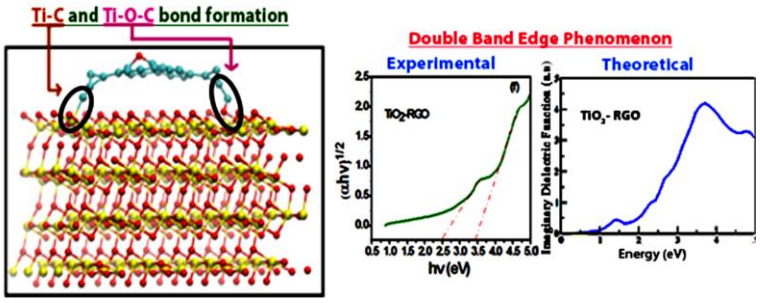

A Possible Mechanism for the Emergence of Additional Band Gap due to Ti-O-C Bond in TiO_2 - Graphene Hybrid System for Enhanced Photodegradation of Methylene Blue under Visible Light

Sima Umrao[†, #], Shiju Abraham[†, #, £, ‡], Frank Theil[£, ‡], Shobhit Pandey[¥], Valerian Ciobota[£], P. K. Shukla[€], Caroline J Rupp[θ], Sudip Chakraborty[λ], Rajeev Ahuja[λ], Jürgen Popp[£, ‡], Benjamin Dietzek[£, ‡,*], Anchal Srivastava[†,*]

[†]Department of Physics, Banaras Hindu University, Varanasi, 221005, India.

[£]Institute of Physical Chemistry and Abbe Center of Photonics, Friedrich-Schiller-University, Helmholtzweg 4, D-07743, Jena, Germany.

[‡]Leibniz-Institute of Photonic Technology Jena (IPHT), Albert-Einstein-Str. 9, D-07745, Jena, Germany.

[¥]Department of Metallurgical Engineering, Indian Institute of Technology-B. H. U., Varanasi, 221005, India

[€]I.T.S. Engineering College, Greater Noida, 201308, India

[θ]Departamento de Física, Universidade Federal de Santa Maria, 97105-900, Santa Maria, RS, Brazil

[λ]Condensed Matter Theory Group, Department of Physics and Astronomy, Uppsala University, Box-516, Sweden

[*] **Corresponding authors:**

Address correspondence to anchalbhu@gmail.com, benjamin.dietzek@ipht-jena.de

Abstract

Here we report experimental and theoretical study of two TiO_2–graphene oxide (TG) and TiO_2–reduced graphene oxide (TR) composites synthesized by a facile and ecological route, for enhanced visible light (~470nm) photocatalyc degradation of Methylene Blue (MB) (99% efficiency), with high rate constant value (1800% over bare TiO_2). TG couples TiO_2 nanopowder with Graphene Oxide (GO) while TR couples it with reduced graphene oxide (RGO). The present study, unlike previous reports, discusses never before reported double absorption edges obtained for both TG (3.51 eV and 2.51 eV) and TR (3.42 eV and 2.39 eV) composites, which marks the reason behind feasible visible light (2.56 eV) induced photocatalysis. TiO_2 domains in the composites dominate the higher band edge, while GO/RGO domains explain the lower band edge. Formation of Ti-O-C bond in both TG and TR drives the shifting up of the valence band edge and reduction in band gap. Further, these bonds provide a conductive pathway for charge carriers from TiO_2 nanopowder to the degrading species via the GO/RGO matrix, resulting in decreased charge carrier recombination in TiO_2 and enhanced efficiency. To attest that the developed theory is proof-positive, density function theory (DFT) calculations were performed. DFT obtained energetics and electronic structures support experimental findings by showcasing the play of Ti-O-C bond, resulting in double band edge phenomenon in composites. Finally, the mechanism behind MB degradation is discussed comprehensively and the effect of weight percent of GO/RGO in composite on rate constant and photodegradation efficiency has been studied experimentally and explained by developing analytical equations.

Keywords: Photocatalytic activity, Titanium dioxide nanopowder, Reduced graphene oxide, Ti-O-C bond, Additional band edge.

Introduction

Hazardous waste management of organic dyes like Methylene blue (MB), rhodamine B, crystal violet through photodegradation has remained a never diminishing area of research.[1-3] Heterogeneous photocatalysts have a commendable efficiency to degrade organic pollutants, and down this line, TiO_2 is one of the most exhaustively studied material owing to its excellent photo-functional properties, strong oxidizing power, absence of toxicity, long term photo and chemical stability, high refractive index and low production cost.[1, 4-7] Holistic reports showcasing photodegradation of MB via reclusive use of TiO_2 are present, but it is well understood that TiO_2 alone fails to achieve high photocatalytic efficiency, because of its compromised quantum efficiency, due to relatively brisk recombination of electrons and holes, adversely affecting the surface redox reaction.[8] Further TiO_2 is activated only by ultraviolet light (<385 nm) as its band gap lies in UV light energy range, which constitutes only about 3–5% of the solar spectrum.[9] Practically, this factor strongly limits the use of solar spectra as a light source for photocatalysis purpose. This limitation can be circumvented by tailoring the absorption capacity of TiO_2 in the visible range, which constitutes about 50% of the energy of the whole solar spectrum. The wide band gap of TiO_2 photocatalyst can be modified to extend its photoresponce into the visible region for degradation of organic dyes in several ways, including coupling with noble metals,[10-12] quantum dots,[13, 14] non-metals doped semiconductors,[6] carbon nanotubes (CNTs)[15, 16] and fullerenes.[17] Further, reports attest that such composite formations,[12, 18-20] especially with carbon materials can inhibit the electron-hole pair recombination, thereby enhancing the photocatalytic performance of TiO_2.[15, 21-23]

Among the various carbon nanostructures, graphene and its derivatives, GO and RGO have captured much attention, owing to its modified optoelectronic properties, high surface area, superior electron mobility, lower cost and the easy chemical modification to change surface properties which is favorable for composites fabrication.[24-27] Therefore, the combination of TiO_2 and graphene is much

promising as it simultaneously possesses excellent absorptivity, transparency, conductivity and reachability, which could assist effective photodegradation of pollutants.

There is a pool of reports showing the enhanced photocatalytic activity of TiO_2 nanoparticles with graphene composites for the degradation of organic molecules and photocatalytic splitting of water under UV light.[22, 28-38] Enhanced photocatalytic activity was attributed to the synergetic effect between graphene and TiO_2 nanoparticles, because graphene acts as an excellent electron acceptor and transporter, the Ti-O-C bond open up an easy path for charge transfer which remarkably decreases the recombination of electron–hole pairs.[3] Although claiming good efficiency, many of these reports are based on usage of un-ecological UV light and suffer from low kinetics (k value).[28-30]

Realizing the importance of efficient visible light photodegradation, there are few reportes which show enhanced photocatalytic activity of TiO_2-GO/RGO composites under visible light.[39-42] The results and application part is well comprehended in numerous articles for TiO_2 – graphene based composite; some of which attest the formation of Ti-O-C bond in such composites,[43] but there are none which provide a clear explanation for the mechanism behind the enhanced photocatalytic effect. To do a meticulous study of the reason behind successful visible light MB degradation using such composites, we report two chemically bonded TiO_2 nanopowder composites, out of which one couples TiO_2 nanopowder with GO and other with RGO using a facile synthesis route. Uniquely using FT-IR analysis, the existence of Ti-O-C bond in between TiO_2 and GO/RGO is confirmed. Because of such bond formations, never before discussed double absorption edges are obtained for both TG (3.51 eV and 2.51 eV) and TR (3.42 eV and 2.39 eV) composites. The TiO_2 domains dominate the higher end of range, while GO/RGO domains explain the lower end of range. Again the effect of Ti-O-C bond mark the reason behind the depression of higher value compared to bare TiO_2 (3.68 eV) and increase of lower end of range compared to pure GO/RGO (2.10 eV/1.83 eV). Such two absorption edges were earlier reported in Graphene-*h*-BN system.[44] The existence of such double band edges in our

composites is the novel reason behind the possibility of photocatalytic degradation upon irradiation with 470 nm visible light.

To provide concreteness to our developed understanding, theoretical modeling of optical spectra based on density functional theory (DFT) and utilizing the projector augmented wave method (PAW) implemented in the VASP (Vienna *ab-initio* Simulation Package) program for the theoretical prediction of the energetics and the electronic structure of the individual systems GO, RGO and TiO_2 along with the composites of GO and RGO with TiO_2 was performed. A comparable trend has been found between the experimentally and theoretically obtained optical responses, attesting multiple absorption edges being present in the composites, with similar trend in the band edge range when compared with reclusive TiO_2 and GO/RGO, while as expected only single absorption edge is obtained for TiO_2, GO and RGO separately. Further the DFT obtained structure confirms the presence of Ti-O-C bond in exact correspondence to the data obtained experimentally via FT-IR, whose formation due to the bonding between the free electrons on the surface of TiO_2 with some unpaired $\pi-$ electrons, shifts up the valence band edge and reduces the band gap. Simultaneously, in harmony to experimental results, better photo-efficiency in case of TR than TG is confirmed via theoretical modelling, owing to better bond formation in case of modelled TR, compared to TG. This is further supported by greater band edge shift and even greater reduction in band gap as expected.

For a diligent study, the effect of the ratio of the two components, weight percentages of GO/RGO in both TG and TR composites have been studied. Photocatalytic investigation on the degradation of MB using, reclusive TiO_2, TG composites (both 5:1 wt% (TG1) and 2:1 wt% (TG2)) and TR composites (both 5:1 wt% (TR1)and 2:1 wt% (TR2)) has been accomplished in this work. The composites under normal visible light (470 nm) show astonishing photodegradation efficiency in comparison to bare TiO_2 owing to the play of Ti-O-C bond formation as discussed above. Further the composites are exalted by high rate constant. The mechanism behind MB degradation is discussed

comprehensively and an analytical model to explain the effect of ratio of concentration of GO/RGO in composite on rate constant has been developed. Further our TR2 composite synthesized by the proposed fast, facile, ecological and economical route, achieves astonishing high MB degradation efficiency of 99% exalted by a 1800% increase in the photocatalytic degradation rate constant value in contrast to bare TiO_2.

Experimental Section

Materials

They include titanium (IV) butoxide, ($C_{16}H_{36}O_4Ti$, Sigma-Aldrich Chemicals Pvt Limited, Germany, purity ≥ 97%), graphite flakes (1-2 mm, NGS Naturgraphit GmbH, Germany), potassium permanganate ($KMnO_4$, ≥99.0%, Fluka), ethanol (CH_3CH_2OH, ≥98% Sigma-Aldrich, Germany), ammonia solution, H_2SO_4, H_3PO_4, H_2O_2 and H_6N_2O.

Preparation of Graphene Oxide

GO was synthesized via an improved Hummers method.[45] Briefly, a 9: 1 ratio of concentrated H_2SO_4 / H_3PO_4 was added to 2 g of graphite flakes and 12 g (76 mM) of $KMnO_4$. The mixture was isothermally stirred for 12 h at 50° C. Further the mixture was cooled to the room temperature and subsequently the reaction was quenched by adding approximately 270 mL of ice with 2 mL of 30% H_2O_2. This obtained mixture was then filtered and centrifuged. The solid material was washed with distilled water, 30% HCl and ethanol until a pH≈ 7 was attained and then dried at 80° C in oven. Finally the desired GO dispersion was procured by continuous ultra-sonication for an hour.

Preparation of Reduced Graphene Oxide

RGO was synthesized by reducing the above as obtained GO with the aid of hydrazine hydrate solution (H_6N_2O) as the reducing agent.[46] Briefly, 1000 ml (0.25 mg/mL) solution of as synthesized GO in double distilled (DD) water was kept for ultra-sonication for an hour, to obtain a light yellowish

homogeneous solution. Further 3.92 mL of ammonia solution (25%) was added to the above obtained GO solution to achieve a pH≈10. Thereafter, 700 µL of H_6N_2O was added and the solution was kept under ultra-sonication at a temperature of 80° C for three hours, followed by magnetic stirring at 95°C for 2 hrs. In the final step, the yellowish GO solution turns black on reduction. The solution is then filtered followed by washing with DD water and drying at 80° C.

Preparation of TiO_2 Nanopowder

TiO_2 nanopowder was prepared using sol–gel method[13] employed with slight modifications. Typically, the solution A was prepared by dissolving 17 mL of $Ti(OBu)_4$ (50 mM) in 40 mL of absolute ethanol. Solution B was obtained by mixing 3 mL of concentrated HNO_3, 35 mL of absolute ethanol and 15 mL of de-ionized water. The solution B was mildly stirred and subsequently added drop wise to solution A over a time span of 25 minutes. This obtained mixture was further stirred for 90 minutes and left untouched for 30 hrs. This resulted in light white TiO_2 gels, which were dried at 200° C for 6 hrs. Ultimately the obtained pale yellow nanopowder was used for subsequent characterizations and photocatalytic measurements.

Preparation of Composites

For the preparation of composites, 200 mg of TiO_2 nanopowder was well dispersed in 200 mL of ethanol (96%) by sonication for an hour at ~50° C. Similarly, GO as well as RGO dispersions (1 mg/mL) were taken in ethanol (96%). The four combinations of composite materials were prepared by mixing 50 mL of TiO_2 dispersion (1 mg/mL) with 10 and 25 mL dispersion (1 mg/mL) of GO as well as RGO. The composite solutions were sonicated for an hour at~70° C and then dried at 45° C. The solid materials thus obtained are abbreviated as TG1 (TiO_2:GO=5:1 wt.%); TG2 (TiO_2:GO=2:1wt.%); TR1 (TiO_2:RGO=5:1 wt.%) and TR2 (TiO_2:RGO=2:1wt.%).

Characterization

The morphology of the as synthesized samples was investigated using scanning electron microscopy (SEM) on a JEOL – Model JSM6300F-SEM instrument and transmission electron microscopy (TEM)

using a FEI – Tecnai-20 electron microscope. The crystalline structures of GO, RGO, TiO_2, TG and TR composites were characterized by X-ray diffraction (XRD) (diffractometer system-XPERT-PRO) using Cu-$K_{\alpha 1}$ radiation (λ=1.5405980 Å). In Brunauer-Emmett-Teller (BET) measurements, Nitrogen adsorption/desorption isotherms were measured at 77 K using the Autosorb 1-C instrument from Quantachrome Instrument Corp., USA. Raman measurements were performed on a micro-Raman setup (HR LabRam inverse system, JobinYvon Horiba). The 532 nm line from a frequency doubled Nd:YAG laser (Coherent Compass) was used as excitation wavelength. Fourier transform infrared spectra (FTIR) of the samples were recorded using a Perkin Elmer Spectrum 65, FT-IR spectrometer. Photoluminescence (PL) spectra were measured on a fluorescence spectrophotometer (PerkinElmer) with an excitation wavelength of 300 nm. The EIS measurements were carried out on a PARSTAT 2273 potentiostat/galvanostat (Advanced Measurement Technology Inc., NPL, Delhi) by using three-electrode cells. The dye degradation level was measured using a UV/VIS/NIR Spectrophotometer (JASCO-V-670, with PMT and PbS detectors).

Computational Methodology

The electronic structure calculations of the model systems have been performed based on the density functional theory.[46, 48] The projector augmented wave method (PAW) implemented VASP (Vienna *ab-initio* Simulation Package) program[49, 50] is used throughout for the theoretical prediction of the energetics and the electronic structure. The Perdew-Burke-Ernzerhof (PBE) type of generalized gradient approximation (GGA) has been employed as the exchange-correlation functional[51, 52] for the structural optimization of the structures. It is worth to mention here that the generalized gradient approximation (GGA) tends to underestimate while local density approximation (LDA) tends to overestimate the binding energies. The Brillouin zone has been sampled by 3x3x1 k-mesh using Monkhorst-Pack scheme and the optimal energy cut off of has been used for individual systems of GO, RGO and TiO_2 surface, while for the composite systems Gamma point have been used. For the surface calculations, we have used vacuum of 15 A° in z direction in order to avoid the quenching of wave

functions for all the isolated systems and for the nanocomposites the vacuum was 30 A°. A denser k-mesh has been used to produce the density of states and the smearing width is 0.05 eV. All the structures are optimized until the Hellman-Feynman forces acting on them reduce to 0.005 eV/A°. For the electronic relaxation conjugate gradient algorithm is being considered.

Photocatalytic Activity Test

All the four composites were separately dispersed in absolute ethanol (1mg/mL) by ultra-sonication. 10 ppm MB solution was prepared by dissolving 10 mg of MB powder in 1000 mL of distilled water. For the optimization of the individual composites, the catalytic measurements were carried out in three different proportions of MB and catalyst (CAT). The combinations of catalyst (TiO_2), co-catalyst (GO or RGO) and distilled water (DW) is used in the work are as listed below:

(MB solution in DW (10 mg/1000 mL) =2800 µL) + (CAT solution in Ethanol (1mg/mL) =87.5 µL) + (DW=612.5 µL) ------ P1

(MB solution in DW (10 mg/1000 mL) =2800 µL) + (CAT solution in Ethanol (1mg/mL) =175 µL) + (DW=525 µL) --------- P2

(MB solution in DW (10 mg/1000 mL) =2800 µL) + (CAT solution in Ethanol (1mg/mL) =350 µL) + (DW=350 µL) --------- P3

All the three solutions were then irradiated (central wavelength at 470 nm) under constant stirring using LED-torches (power ~ 0.1 mW/mm^2, Innotas Elektonik, GmbH Germany). UV-Vis absorption spectroscopy was used to study the variation in the absorption maximum of MB. For every hour the absorption measurement was taken and the catalytic degradation was continued up to five hours.

Results and Discussion

Structure and Morphology of TiO_2 and TiO_2- GO/RGO Composites

We systematically investigated the quantitative effect of GO/RGO on photocatalytic activity and band gap modification of as synthesized composites. In the beginning, all samples were characterized both structurally and spectroscopically. The XRD patterns of GO, RGO, TiO_2, TG, and TR are shown in Figure S1 (see in supporting information). In the diffraction pattern of GO, the peak around $2\theta = 10.62°$ corresponds to the (001) reflection (interlayer spacing of 0.83 nm), while the other peak at ~24° having lower intensity compared to the before said peak, is due to short-range order in the stacked graphene like sheets with spacing around 0.36 nm. The diffraction peak of RGO at 24.04° corresponds to the (002) reflection, with d-spacing of 0.37 nm. XRD patterns of TiO_2 nanopowder shows six distinct diffraction peaks at 20.78°, 25.1°, 30.39°, 37.94°, 48.21°, and 54.15°. These can be indexed respectively as (102), (101), (101), (004), (200), and (105) planes of TiO_2 (JCPDS No. 21-1272) having fcc crystal structure. Among the above mentioned peaks, the small obtuse peak around 30.39° corresponds to the rutile (R) phase, while other peaks denote the anatase (A) phase of TiO_2. The diffraction peak at around $2\theta = 20.78°$ corresponds to the (102) reflection for Ti_4O_7 phase of titanium oxide (JCPDS No. 18-1402). The presence of broad peaks and the absence of unidentified peaks confirm the small size, and high purity of the prepared nanopowder. Notably, in the diffraction pattern of TG, the sharp peak of GO become less intense, suggesting the disruption of the GO layers due to formation of partially reduced GO structure and the formation of composite material itself. Furthermore, it can be found that the XRD pattern of the TG and TR, show peaks which are similar to the diffraction pattern of TiO_2. This indicates that the anatase phase is predominant in the composite samples. The XRD pattern of TR showcases clear peaks of pure TiO_2, but the peak at 25° in TiO_2 was broadened, due to its superimposition with the diffraction peak of RGO at 24.04°.

The morphology of TiO_2, TG and TR were characterized by using TEM and SEM. Fig. 1(a-d) shows the TEM images of TiO_2 and TG, whereas Fig. 1(e-f) represents SEM images of TR. From Fig. 1(a) it is clear that the TiO_2 nanopowder consists of 2-15 nm sized TiO_2 particles. Furthermore, the higher magnified image (Fig. 1(b)) of the same sample delineates several crystal planes of TiO_2

nanopowder which are randomly oriented across the particles. Fig. 1(c) represents the micrograph of TG, where clearly TiO_2 nanopowder can be seen uniformly decorated on the surface of GO. Further, well resolved adjacent image (Fig. 1(d)) depicts the crystal planes of TiO_2 nanopowder on GO surfaces. From the SEM images of TR (Fig. 1(e) and 1(f)) it is visible that the TiO_2 nanopowder is well attached to the RGO surfaces. Thus, both TEM and SEM images (Fig. 1(c-f)) attest the intimate contact between TiO_2 nanopowder with GO and RGO sheets, which probably constitutes the basis for electronic interactions between the components.[53] These results further reveal that GO and RGO inhibit the aggregation of TiO_2 nanopowder. The specific surface area of TiO_2 nanopowder is measured by Brunauer-Emmett-Teller (BET) analysis, which showed the presence of high specific surface area of TiO_2 nanopowder of around~ 250 m^2/g, attesting the inhibition of TiO_2 agglomeration (see in supporting information). Additionally the test also provided results for average pore diameter, which in present case came out to be of 0.24 nm. The Raman investigation (See supporting information, Figure S2) supports the successful synthesis of GO, RGO, TiO_2, TG and TR. Further Fourier transform infrared (FT-IR) spectra of the TiO_2 nanopowder, TG and TR composites were measured to study the different functional groups and chemical bonds present, such as Ti-O-Ti vibrations and Ti-O-C vibrations in the system (Figure S3, See supporting information), which were further confirmed by DFT calculations.

In order to study the formation of chemical bonds Ti-O-C and Ti-C after loading TiO_2 with GO and RGO, the interactions between TiO_2 and GO/RGO are also investigated by the analysis of XPS results of TG and TR as shown in Figure 2. The core level O1s XPS spectra of TG and TR are given to prove the existence of Ti-O- C (Figure 2a, d). The main peaks centered at 529.08 and 530.09 eV correspond to Ti–O–Ti (lattice O).[54] The peaks with higher binding energy located at 530.02 and 530.89 eV are attributed to the Ti–O–C for both TG and TR respectively.[54] The other peaks centered at 532.11 eV and 532.89 eV correspond to Ti-OH and C-O groups for TG.[54] Furthermore, in case of TR, the peak cantered at 531.65 eV was attributed to the C–O groups. Figure 3c shows the core level

spectra of C 1 s for TG hybrid with its peak positions observed at binding energies of 284.18, 284.94 and 287.44 eV corresponding to C–C, C=O, and C–OH bonds, respectively.[55] For the TR hybrid (Figure 2f), three peaks centered at 284.21, 285.27, and 287.10 eV correspond to C–C in aromatic rings, C=O, and C-OH groups, respectively.[2] Additionally, in TR, another peak at 282.5 eV (Ti-C) was observed, which could be because of the chemical bonding between titanium and carbon.[55] Figure 2b and e showcase the chemical states of Ti(IV) species in TG and TR respectively. The Ti 2p core levels can be deconvoluted to a doublet (Ti 2p3/2 and Ti 2p1/2), recording a binding energy difference (ΔE_{BE}) of 5.61 and 5.71 eV for TG and TR respectively, which indicates the presence of normal states of Ti(IV), and is consistent with the earlier report.[56] The binding of GO/RGO and TiO_2 may be advantageous for the transport of electrons through TG and TR hybrids. However, the increase in (ΔE_{BE}) of TR reveals that the interaction between TiO_2 and RGO is better than TiO_2 and GO.

Modified Optical Band Gap Study

UV-Vis absorption spectrum and PL spectra of the TiO_2, TG and TR were measured in order to investigate the optical energy gap of the samples. After addition of GO/RGO, the synergistically interacting GO/RGO matrix modifies the electronic band gap structure of TiO_2 and opens up an energy level between conduction and valence band, as a consequence of which the band gap energy of TiO_2 is reduced and additional band edge originates. This result is explained analytically and supported by similar double band edge structures obtained for composites through DFT calculations.

Experimental Study for Optical Band Gap

To determine the optical band gap, we plotted the modified Kubelka-Munk function, i.e., $[\alpha h\nu]^{1/2}$ (α is the absorption coefficient, h is Planck's constant, ν is the light frequency) versus the photon energy of the exciting light ($h\nu$). The absorption spectrum of bare TiO_2 (Fig. 3(a)) shows one absorption edge corresponding to a band gap of 3.68 eV. The absorption spectrum of GO and RGO show a weak absorption band of about 2.10 eV and 1.83 eV respectively (Fig. 3(b) and 3(c)). Uniquely, the

absorption spectrum of TG and TR composites are showing double absorption edges. For TG, the first absorption edge corresponds to an optical band gap of 3.51 eV, which must be driven by TiO_2 domains in the composite. The value as speculated is less than bare TiO_2 (3.68 eV), signifying the effect of synergistically interacting TiO_2 and underlying GO matrix, effecting the TiO_2 domains, caused by the Ti-O-C bond formation which is confirmed by FT-IR spectra. In case of TR composites, this higher band edge value reduces to 3.42 eV, owing to enhanced interactions between TiO_2 and RGO matrix. This is attested by FT-IR analysis results, showing improved Ti-O-C bonds signals in case of TR composites, in contrast to TG composites. The second (lower) absorption edge is obtained at 2.51 eV and 2.39 eV for TG and TR composites respectively. The prominent driving force behind these absorption edges are the GO and RGO domains in case of TG and TR composites, respectively. Again as expected the values 2.51 eV (TG) and 2.39 eV (TR) are greater than that of pure GO (2.10 eV) and RGO (1.83 eV), which is a direct effect of TiO_2 on the GO and RGO matrix, via Ti-O-C bond formation. Further, quenching in photoluminescence spectra of the TiO_2 nanopowder after addition of GO and RGO support the reduction in active band gap of TiO_2 (see supporting information, Figure S4). The above incisive explanation for multiple band gaps observed in TG and TR results evinces the pioneer result of achieving the degradation of MB under normal visible light. This exalts these composites as a much better candidate, due to their ecological functioning compared to earlier UV light based MB degradation using TiO_2 composites.

Computational Study of the Optical Band Gap

In order to support the experimental results outlined above, we have calculated the optical spectra based on density functional theory (DFT) for the individual systems GO, RGO and TiO_2 along with the composite systems of GO and RGO with TiO_2 (Figure 4 and 5). The anatase TiO_2 surface, which is a tetragonal crystal structure, has been constructed with the slab size 4x4x4, with the interlayer distance as 3.95 A°. The optical gap of any system is directly related to the first absorption peak of optical spectra. Therefore, determining the optical response is quite intuitive from the optical gap perspective.

The visible light driven photocatalytic activity of the experimentally synthesized TiO_2 nanopowder, TG and TR composites have been compared from the optical spectra analysis, which is an artifact of the optical absorption gap of these materials. The calculated optical spectra can be compared to the UV-VIS spectra of experimentally synthesized TiO_2 nanopowder, GO, RGO and their respective composites with TiO_2 as depicted in Figure 4 and Figure 5. A comparable trend has been found between the experimentally and theoretically obtained optical responses. The absorption peak strength can also be varying if one goes from individual system to the composite systems. We have started calculating the composites by introducing 3 A° distance between surface and adsorbate. This distance has been chosen to be between physisorption and chemisorption binding. It has been found that in the relaxed structures, this distance is getting decreased to 2.4 A° and 2.1 A° for TG and TR system respectively as the shortest distance between adsorbate and surface. It leads to the inference that RGO is binding more with anatase TiO_2 than GO, hence the charge transfer between the surface and the adsorbate is more prominent in case of TR than TG, which is in agreement with experimental findings. This influences the optical absorption peak for the nanocomposites as well. We can assume that the formation of Ti–O–C bond are due to the bonding between the free electrons on the surface of TiO_2 with some unpaired $\pi-$ electrons, which then shifted up the valence band edge and reduced the band gap. Hence attesting the experimental findings, multiple absorption edges have been found in the nanocomposites of TG and TR, whereas single absorption edge is prominent for individual systems of TiO_2, GO and RGO.

Enhanced Photocatalytic activity

To study the effect of wt. % ratio of TiO_2: GO/RGO on both photodegradation efficiency of MB and photocatalytic rate constants, five as synthesized samples, abbreviated as bare TiO_2 nanopowder, TG1, TG2, TR1, TR2 (for details see Sec. 2.5) were analyzed for their photocatalytic behavior in five equal time intervals (each of 60 min), under visible light (470 nm) irradiation. The observed change in normalized temporal concentration (C/C_0) of MB during photodegradation is proportional to the

normalized maximum absorbance (A/A_0). Here initial concentration (C_0) is regarded as the concentration of MB after adsorption equilibrium.

Fig. 6 illustrates the measured photodegradation performance of different photocatalysts with varying concentration under the same reaction conditions. Fig. 6 a shows remaining percentage of MB in solution after irradiation of visible light and Fig. 6 b depicts the photodegradation performance of MB with respect to time and it is found that the composites, TG and TR, exhibit faster and better photo degradation capability than pure TiO_2 nanopowder. Multiple concentrations of each of TG1, TG2, TR1 and TR2 were studied for photodegradation of MB (Fig.5c and 6d). Increase in the concentration of the TR composites in MB solution (P1, P2 and P3) improves the photocatalytic activity, while decreased photocatalytic activity is observed upon increasing the concentration of the TG composite (P1 to P3); (For details see Sec. 2.8). The TR2-P3 composite shows the highest photocatalytic activity with an average degradation of MB of 98.72% within 300 min, while with pure TiO_2 nanopowder this value drops down to 36.84% and for GO or RGO, it is ~ 38% for the same period of time. Without the use of a catalyst, the concentration of MB changes slightly both under exposed (around 5% during 300 min exposure) and dark (only 3%) conditions.

Figure 7 summarizes the meticulous comparative analysis of photodegradation efficiency and rate constant of all the four as synthesized TiO_2 composites (TG1, TG2, TR1, TR2), with as synthesized bare TiO_2 nanopowder and earlier reported[26] TiO_2-Graphene composite for MB degradation, carbon nanotubes/TiO_2 nanotubes[15] and M-fullerene/TiO_2 for MO and MB degradation respectively[17]. The Figure 7 clearly shows that the *k* value and photodegradation efficiency of our synthesized composites is high in comparison to earlier reported TiO_2-Graphene composite even they have used UV light having high energy than visible light. For determining the rate constant, the degradation of dye could be assigned to a pseudo-first-order kinetics reaction by linear plot with a simplified Langmuir-Hinshelwood model when C_0 is low.[57] That is

$$\ln (C_0/C) = kt$$

where k is the apparent first-order rate constant.

Clearly both TG (TG1 and TG2) and TR (TR1 and TR2) composites surpass bare TiO_2 in terms of efficiency and rate constant. For TR2 composite, highest k value is 0.0621 min^{-1} (with efficiency ~99%) and for TG2 composite it is 0.0236 min^{-1} (with efficiency ~76%), which is about 1780% and 614% higher than that of bare TiO_2 (36 % efficiency with k value 0.0033 min^{-1}). Clearly both TR1/TG1 have lower rate constant value compared to TR2/TG2 respectively, attesting the enhanced effect of decreasing wt % TiO_2 in both composites on the rate constant. In contrast, the effect of decreased wt% TiO_2 in composites on photodegradation efficiency, is opposite for TG (decrease), than in case of TR (increases). A detailed analytical model explaining probable reasons behind such dependence of rate constant and photodegradation efficiency on the wt % of GO/RGO in TG and TR composites has been provided in the supplementary information (see supplementary information).

Mechanism of Enhanced Photodegradation Efficiency

The schematic (Fig. 8a) illustrates the mechanism of charge transfer from TiO_2 to GO, RGO via the interfaces supported by Ti-O-C bond, which give a path for the charge transfer between TiO_2 to GO/RGO matrix and hinder the recombination of electron-hole pairs. After irradiation of visible light, photoexcitation in TiO_2 is from O-2p orbital on the valance band (VB) to the Ti-3d orbital on the conduction band (CB), generating holes at the O-2p state with a very high redox potential.[58] Due to this high redox potential of the holes, the hydroxyl radicals (•OH) are produced from water, having the potential to degrade the organic pollutants. The photo-generated electrons in the TG or TR photocatalyst can now easily migrate from the inner region to the surface, react with adsorbed O_2 on the surface, resulting in generation of radicals such as $O_2^{\cdot -}$, thereby increasing the overall efficiency. The reaction mechanism behind the degradation of MB by TR composite (also valid for TG composite by replacing RGO with GO) can be expressed as follows:

$$TiO_2\text{-RGO} + hv \rightarrow TiO_2\ (e^-) - RGO + TiO_2\ (h^+) - RGO$$

$TiO_2 (e^-)$ - RGO → TiO_2 – RGO (e^-)

RGO (e^-) + O_2 → RGO + $O_2^{\cdot -}$

$TiO_2 (h^+) + H_2O \rightarrow H^+ + OH^{\cdot}$

$O_2^{\cdot -}$ + $OH^{\cdot}$ + MB → Degrade MB

The enhancement of charge carrier separation clearly results in an increased concentration of more reactive oxidizing species (such as $OH^{\cdot}$, $O_2^{\cdot -}$), which enhances the photodegradation of MB.[25] The typical electrochemical impedance spectra (Fig. 8b) of ITO, TiO_2, TG and TR clearly attest enhanced photocatalytic degradation in TG and TR. Here the impedance spectra in the frequency range varying from 0.01 Hz to 10 kHz was recorded in the three electrode configuration using the catalytic materials as working electrode, Ag/AgCl as reference, platinum as counter electrode and PBS solution (pH 7) containing 5 mM $[Fe(CN)_6]^{3-/4-}$ as the electrolyte. A single semicircle at the high frequency region and a straight line at the low frequency region indicate a mixed charge transfer and charge diffusion process.[59] It is observed that, with the introduction of GO/RGO in TiO_2, though in small amount, the span of semicircle is reduced, which indicates a decrease in both the solid state interface layer resistance and the charge transfer resistance (R_{ct}) on the surface. The R_{ct} values of the TG/TR electrode was much smaller than that of the TiO_2 electrode, which illustrates that TG/TR lead to a much lower charge transport resistance and much higher separation efficiency of electrons and holes, both together resulting in enhanced photocatalytic degradation of MB.

Conclusions

Distilling the above work, we developed two class of chemically bonded TiO_2-GO/RGO hybrids with different weight-percent-ratio using facile, economic, ecological and fast route, exhibiting high photocatalytic activity (for TR2 – 99%) and high rate constant value (for TR2 – 1900% more than bare TiO_2) under visible light. FT-IR analysis confirms the formation of Ti-O-C bond in both TR and TG

composites, resulting in the emergence of new optical band edge in both TG (3.51 eV and 2.51 eV) and TR (3.42 eV and 2.39 eV) composites. Alongside DFT calculations again confirm, both, similar trend for double band edges for composites and the existence of Ti-O-C bond, which shift up the valence band edge and reduce the band gap. Further, these bonds provide a conductive pathway for charge carriers, inhibiting their recombination in TiO_2 (confirmed by EIS and PL spectra), resulting in enhanced efficiency compared to bare TiO_2. Greater narrowing of the band gap and better conductivity in case of TR is observed compared to TG. Theoretically also better binding of RGO with anatase TiO_2, than of GO with the same is acknowledged. The consequence is better photocatalytic response of TR compared to TG composites.

***Conflict of Interests*:** The authors declare no competing financial interest.

■ AUTHOR INFORMATION

Corresponding Authors

Address correspondence to anchalbhu@gmail.com, benjamin.dietzek@ipht-jena.de

■ ACKNOWLEDGEMENTS

The authors express their sincere gratitude to late. Prof. B. P. Asthana, who had initiated this project. The authors are thankful to Andy Scheffel and Dr. Jan Dellith from IPHT, Jena for SEM measurements, Mrs. Anna Schmidt from IPC, Jena for BET measurements, Christa Schmidt from IPHT and Mr. Vineet Srivastava from IIT Kanpur for XRD measurements, Dr. Il-Kwon Oh from KAIST, South Korea for TEM measurements, and Prof. Snajay Kumar from Bio-physics lab, BHU, for PL and some of UV-Vis measurements. The authors are thankful to Dr. Preeti Suman Saxena, Department of Zoology, Banaras Hindu University for providing some of her laboratory facilities. Two of us (SA, JP) are thankful to Deutsche Forschungs-Gemeinschaft (DFG). AS acknowledges CAS program sponsored

by UGC at Department of Physics, B. H. U and DST, New Delhi, India. SU, SA and RKS express their gratitude for the U.G.C. financial assistances. BD and FT gratefully acknowledge funding of the research project 'Photonic Nanomaterials' - PhoNa (Grant No. 03IS210EA) within the framework 'Spitzenforschung und Innovation in den Neuen Ländern' from the Bundesministerium für Bildung und Forschung (BMBF). CR would like to acknowledge CNPq and CAPES for the financial support. SC and RA would like to acknowledge the Carl Tryggers Stiftelse for Vetenskaplig Forskning (CTS), Swedish Research Council (VR), Swedish Energy Agency, and Stiffelsen J. Gust Richerts Minne (SWECO) for financial support. SNIC is also acknowledged for providing computing time.

Author Contributions

S.U. and S.A. equally contributed on this work. A.S. conceived the experiment. S.U. and S.A. contributed to sample fabrication. S.U. carried out UV absorption, PL measurement and FTIR spectra. V.C. carried out the Raman measurements. S.A. and F.T. performed the photocatalytic experiments. B.D. and J.P. discussed regularly the measurement results while conducting the experiments. C.J.R., S.C. and R.A. performed theoretical analysis by DFT. P.K.S. discussed all the optical measurement result. S.P. has corroborated the work with an analytical model for enhanced photocatalytic activity. S.U., S.A., S.P. and A.S. co-wrote the manuscript. All authors discussed the results and commented on the paper.

■ ASSOCIATED CONTENT

Supporting Information Available:

The supporting file includes the RAMAN, FTIR and the XRD diffraction pattern of as synthesized GO, RGO, TiO_2, and composites as well as PL emission spectrum with explanations. This material is available free of charge via the Internet at *http://pubs.rsc.org*.

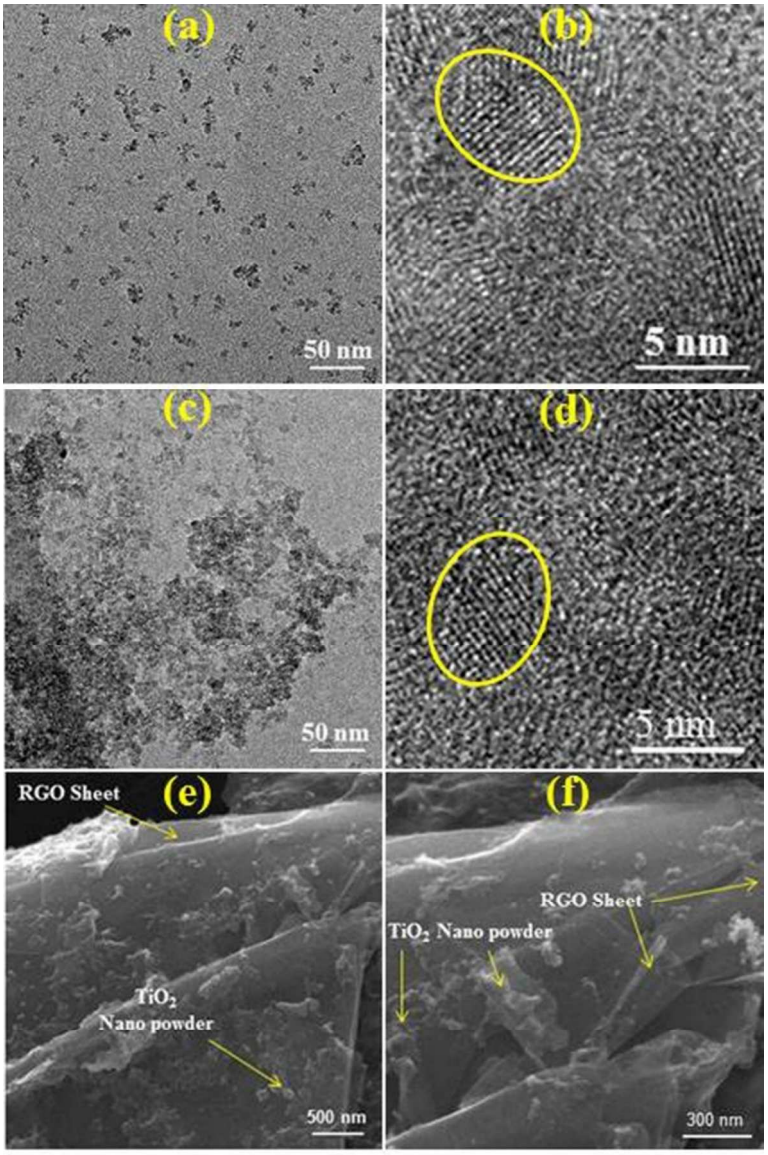

Figure 1. **(a)** TEM images of TiO_2 nanopowder; **(b)** HRTEM image of TiO_2 nanopowder shows several crystal planes randomly oriented across the particles; **(c)** TEM image of TG; **(d)** HRTEM image of TG showing crystal planes. (**e** and **f**) SEM images of TR at different magnifications.

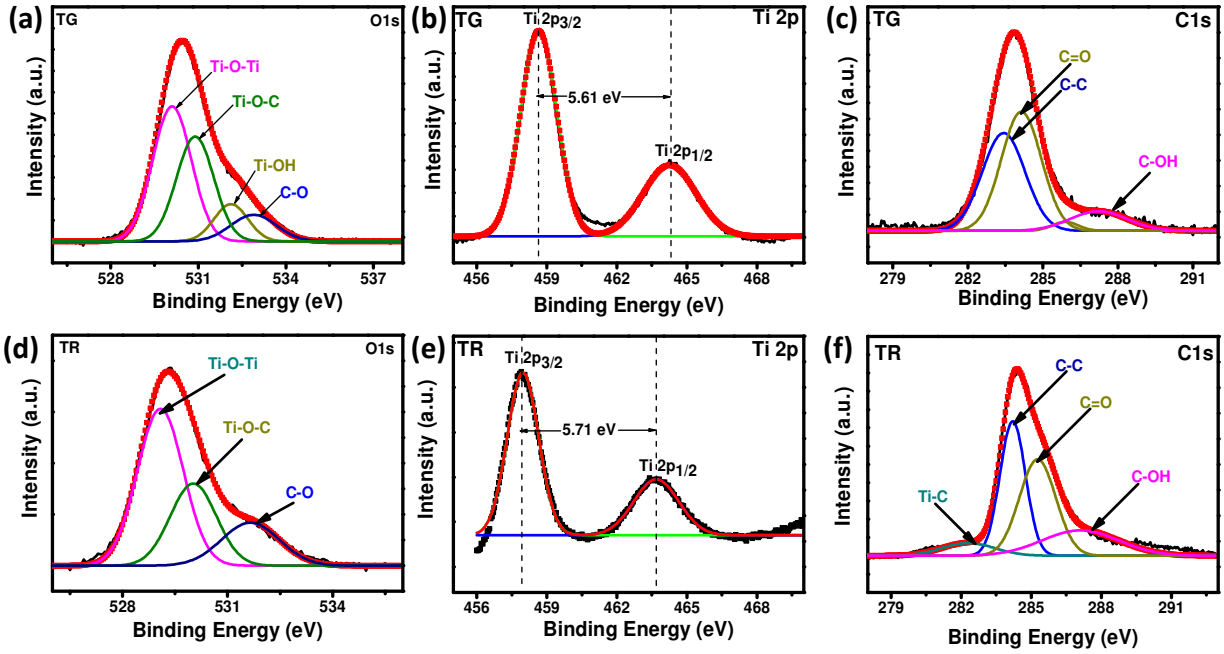

Figure 2. XPS analysis. O1s (a, d), C1s (c, f) and Ti2p (b, e) core level XPS spectra of TG and TR hybrids respectively.

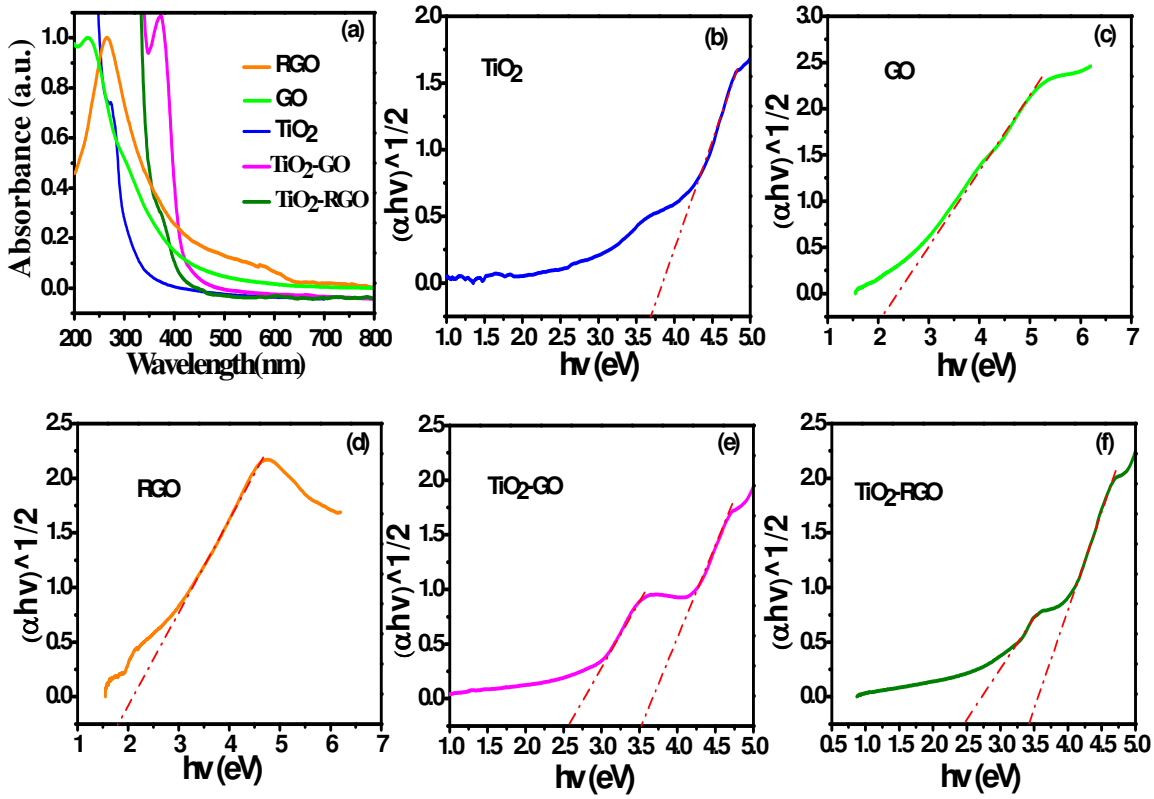

Figure 3. (a) UV-Vis spectra of as prepared TiO_2 nanopowder, GO, RGO, TG and TR composites. The plot of transformed Kubelka-Munk function versus the energy of light for the calculation of Eg, (b), (c), (d), (e) and (f) for as synthesized TiO_2, GO, RGO, TG and TR composites respectively.

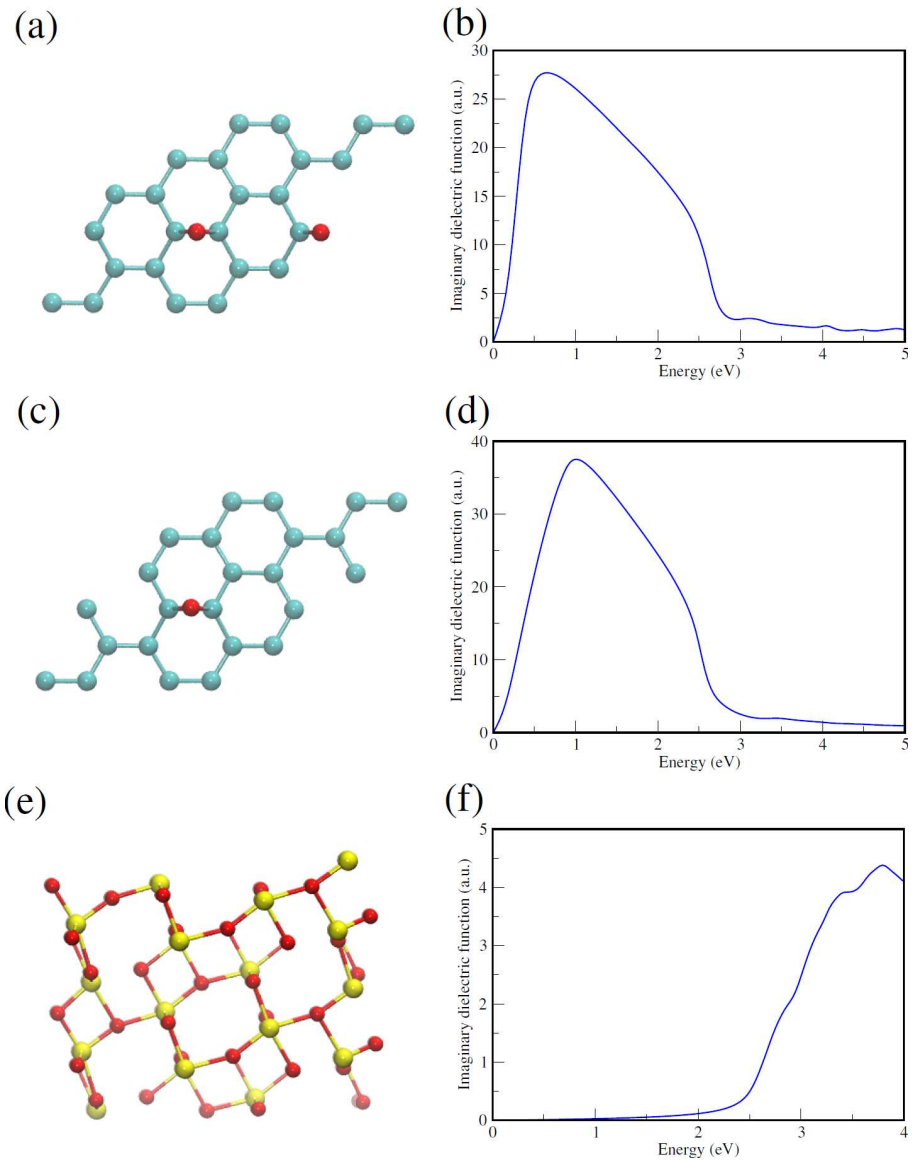

Figure 4. Optimized structures and calculated imaginary dielectric function (a.u.) as an energy for GO [(a) and (b), respectively], RGO [(c) and (d), respectively] and TiO_2 [(e) and (f), respectively]. The cyan, red and yellow balls represent the carbon, oxygen and titanium atoms, respectively.

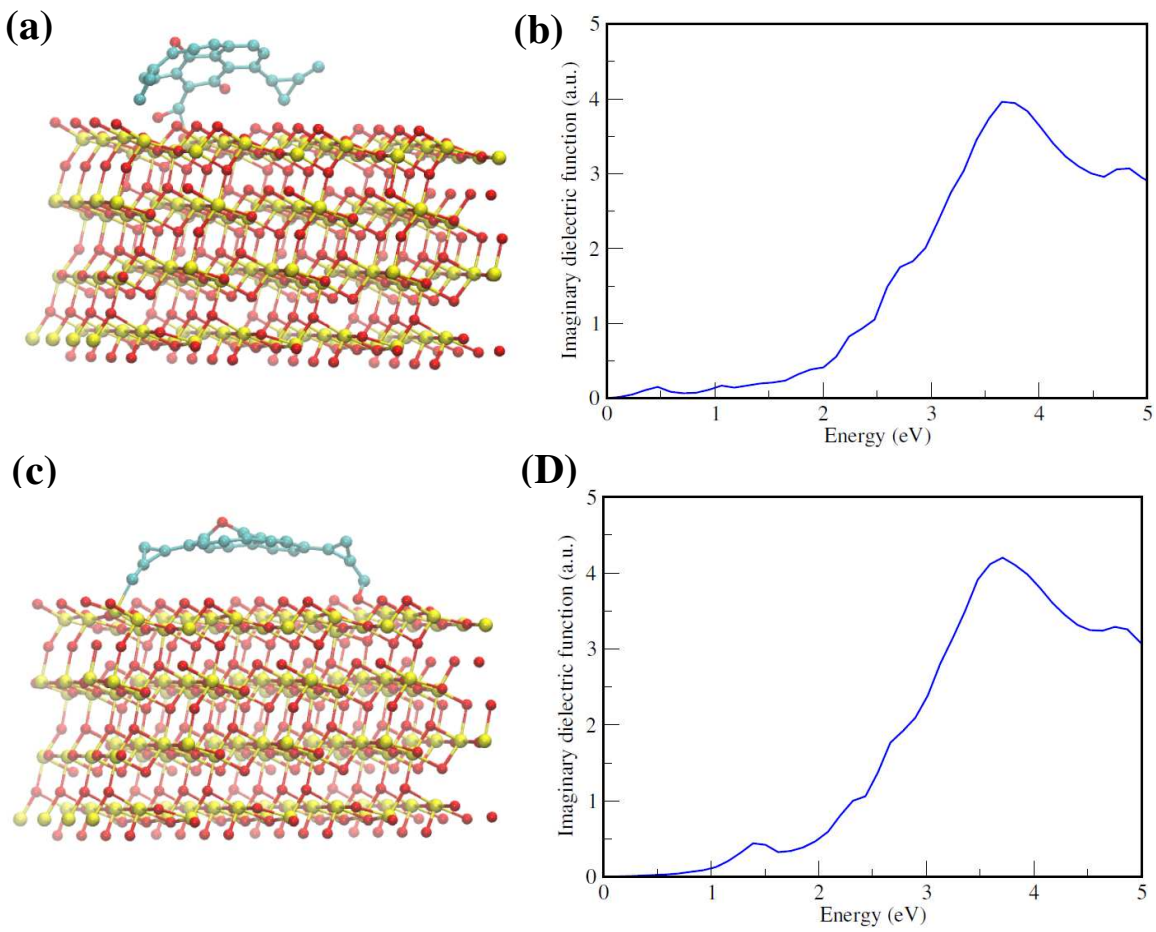

Figure 5. Optimized structure (a) and calculated imaginary dielectric function (a.u.) as a energy (b) for GO+TiO_2 heterojunction. Optimized structure (c) and calculated imaginary dielectric function (a.u.) as a energy (d) for RGO+TiO_2 heterojunction. The cyan, red and yellow balls represent the carbon, oxygen and titanium atoms, respectively.

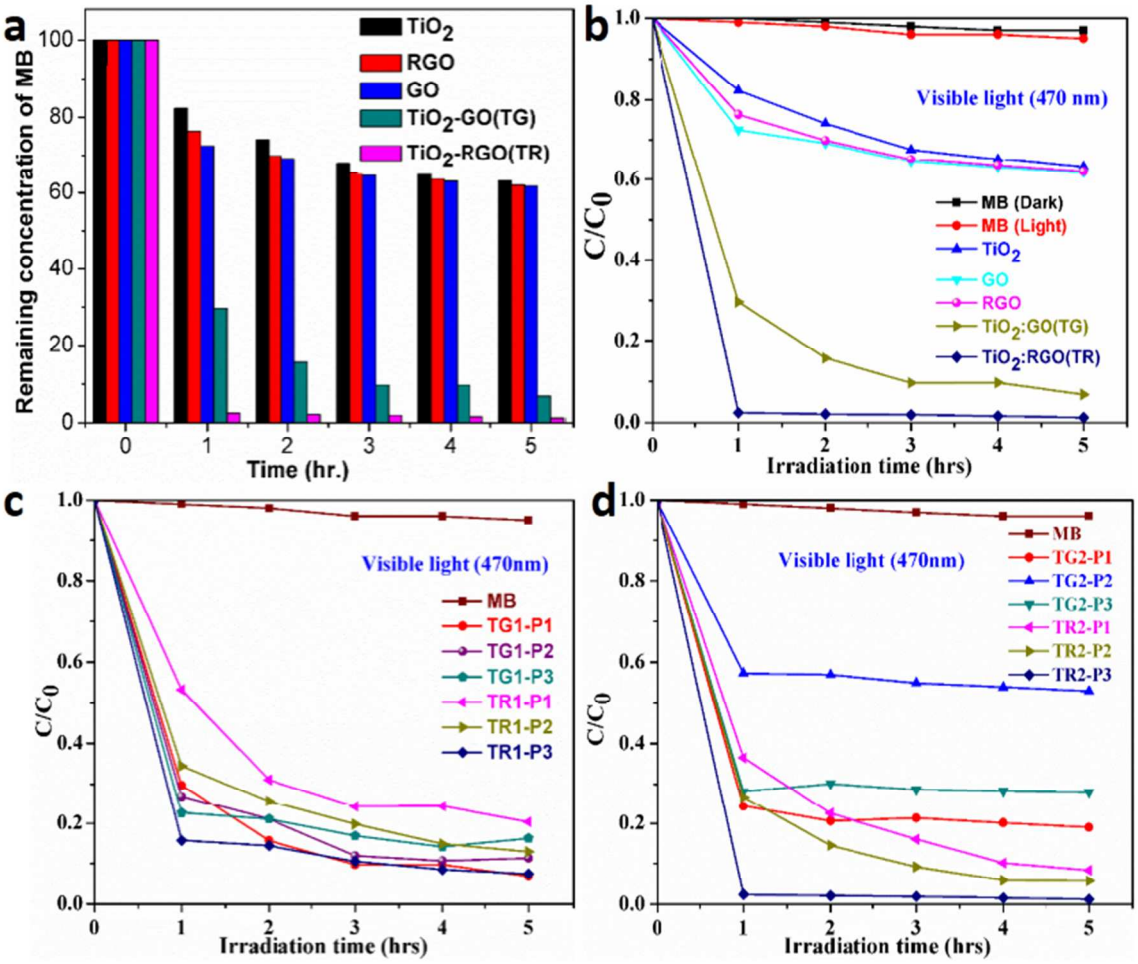

Figure 6. The Bar plot showing the remaining MB in solution after the irradiation of visible light (470nm) over the as synthesized TiO_2 nanopowder, GO, RGO, TG and TR composites (a), In liquid phase maximum photocatalytic degradation of MB under visible light (470nm) over TiO_2, GO, RGO, TG and TR composites (b), photodegardation of MB over TG (5:1) and TR (5:1) (c) and photodegradation of MB over TG (2:1)and TR (2:1) (d) under visible light.

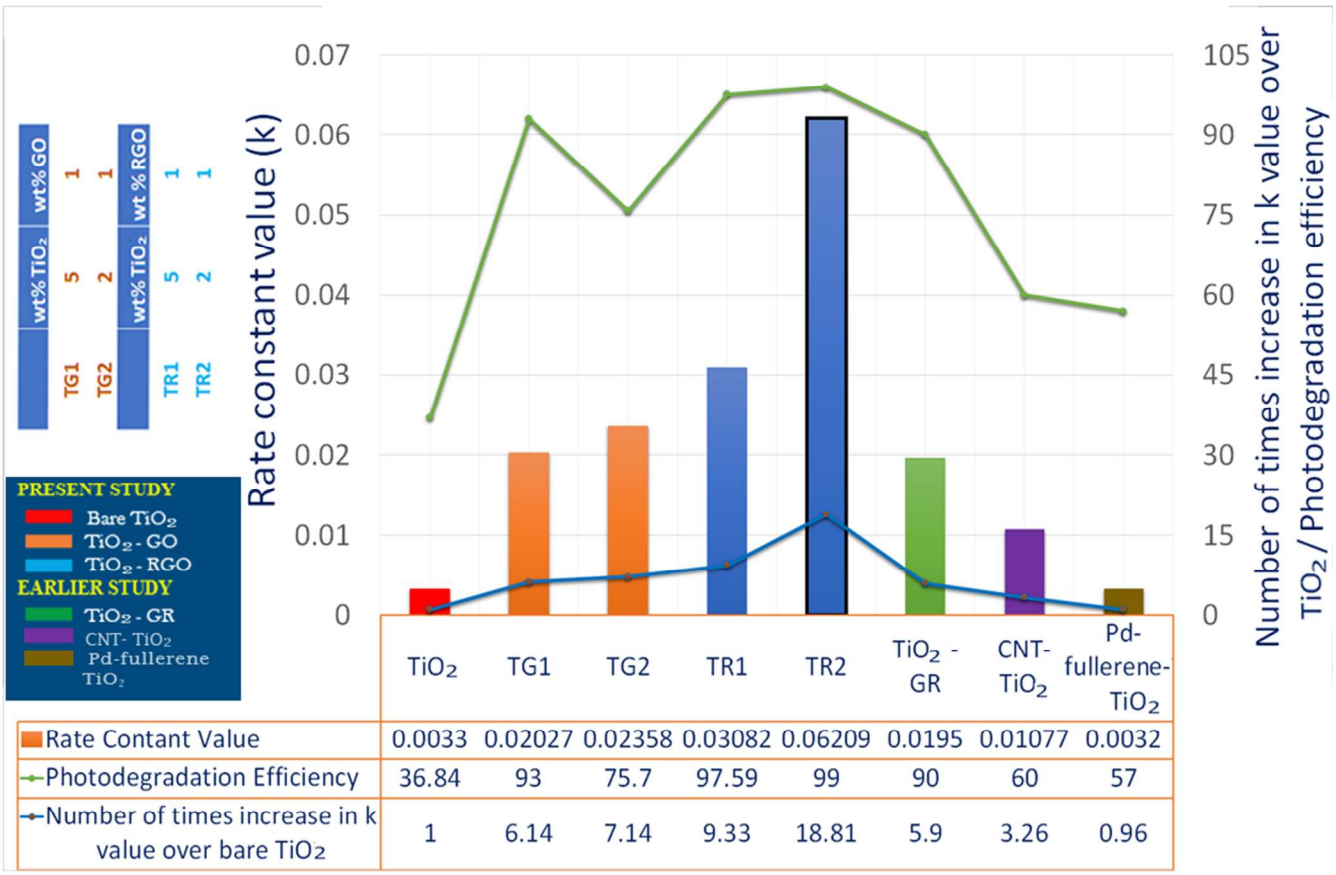

Figure 7. Comparative study of rate constant (k) and photodegradation efficiency of TG and TR composites (present work) vs. bare TiO_2 (present work)/earlier reported TiO_2-graphene composites, CNT-TiO_2 composites and Pd-fullerene TiO_2 hybrids for photocatalytic degradation of methylene Blue.

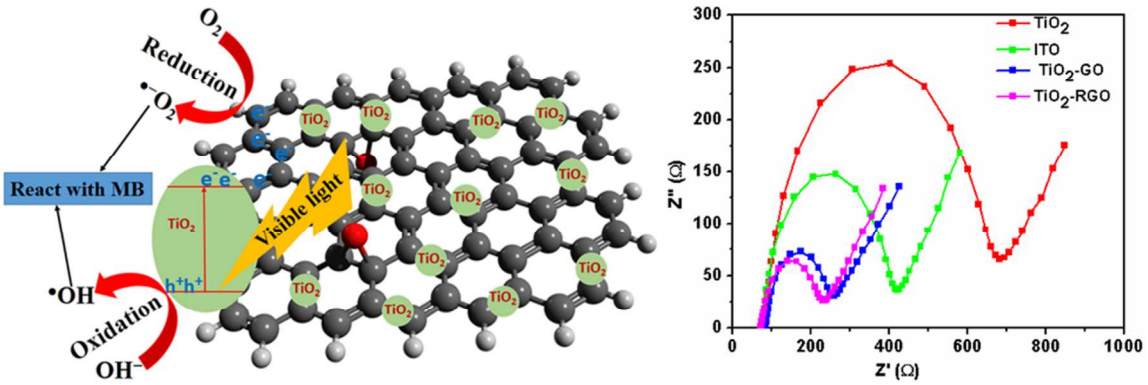

Figure 8. (a) Schematic illustration of enhanced photocatalytic activity of TR Composites by photodegradation of MB under visible light irradiation. (b) EIS changes of TiO_2, TG and TR electrodes. The EIS measurements were performed in the presence of a PBS solution (pH 7) containing 5 mM [Fe(CN)6]3-/4-.

REFERENCES

1. M. A. Al-Ghouti, M. A. M. Khraisheh, S. J. Allen and M. N. Ahmad, *J. Environ. Manage*., 2003, **69**, 229-238.
2. M. R. Hoffmann, S. T. Martin, W. Choi and D. W. Bahnemann, *Chem. Rev*., 1995, **95**, 69-96.
3. A. Fujishima and K. Honda, *Nature,* 1972, **238**, 37-38.
4. H. S. Wahab, T. Bredow and S. M. Aliwi, *Chem. Phys*., 2008, **353,** 93-103.
5. A. Yamakata, T.-a. Ishibashi and H. Onishi, *Chem. Phys*., 2007, **339**, 133-137.
6. Y. Ni, Y. Zhua and X. Ma, *Dalton Trans.*, 2011, **40**, 3689–3694.
7. R. M. D. Hernandez-Alonso, F. Fresno, S. Suarez and J. M. Coronado, *Energy Environ. Sci., 2009*, **2**, 1231-1257.
8. A. L. Linsebigler, G. Lu and J. T. Yates, *Chem. Rev*., 1995, **95**, 735-758.
9. A. Kudo, K. Omori and H. Kato, H. *J. Am. Chem. Soc*., 1999, **121**, 11459-11467.
10. S. Kim, S. J. Hwang, W. Choi, *J. Phys. Chem. B*, 2005, **109**, 24260–24267.
11. X. Zhang, Y. Liu, S.-T. Lee, S. Yang and Z. Kang, *Energy Environ. Sci.,* 2014, **7**, 1409-1419.
12. T. Tong, J. Zhang, B. Tian, F. Chen, D. He, M. An, *J. Colloid Interface Sci.* 2007, **315**, 382–388.
13. E. A. Kozlova, N. S. Kozhevnikova, S. V. Cherepanova, T. P. Lyubina, E. Y. Gerasimov, V. V. Kaichev, A. V. Vorontsov, S. V. Tsybulya, A. A. Rempel and V. N. Parmon, *J. Photochem. Photobiol. A: Chem.*, 2012, **250**, 103, 103-109.
14. X. Yu, J. Liu, Y. Yu, S. Zuo and B. Li, *Carbon*, 2014, **68**, 718-724.
15. M. L. Chen, F. J. Zhang, and W. C. Oh, *J. Korean Ceramic Soc.*, 2008, **45**, 651-657.
16. J. Yu, T. Ma and S. Liu, *Phys. Chem. Chem. Phys.,* 2011, **13**, 3491–3501.

17. Z.-D. Meng, F.-J. Zhang, L. Zhu, C.-Y. Park, T. Ghosh, J.-G. Choi, W.-C. Oh, *MATER. SCI. ENG.*, 2012, **C 32**, 2175–2182.

18. M. Wang, J. Ioccozia, L. Sun, C. Lin and Z. Lin, *Energy Environ. Sci.,* 2014, **7**, 2182-2202.

19. Z. Zhang, C. Shao, X. Li, Y. Sun, M. Zhang, J. Mu, P. Zhang, Z. Guo and Y. Liu, *Nanoscale,* 2013, **5**, 606-618.

20. P. A. DeSario, J. J. Pietron, D. E. DeVantier, T. H. Brintlinger, R. M. Stroud and D. R. Rolison, *Nanoscale*, 2013, **5**, 8073-8083.

21. W. Ren, Z. Ai, F. Jia, L. Zhang, X. Fan and Z. Zou, *Appl. Catal. B: Environ.,* 2007, **69,** 138-144.

22. W. Wang, J. Yu, Q. Xiang and B. Cheng, *Appl. Catal. B: Environ.*, 2012, **119–120**, 109-116.

23. Y. Yao, G. Li, S. Ciston, R. M. Lueptow and K. A. Gray, *Environ. Sci. Tech.*, 2008, **42,** 4952-4957.

24. K.S. Novoselov, A.K. Geim, S.V. Morozov, D. Jiang, Y. Zhang, S.V. Dubonos, I.V. Grigorieva and A.A. Firsov, *Science,* 2004, **306,** 666-669.

25. A.K. Geim, *Science,* 2009, **324,** 1530-1534.

26. K. Krishnamoorthy, R. Mohan and S.-J. Kim, *Appl. Phys. Lett*., 2011, **98**, 244101-244103.

27. T.-F. Yeh, J.-M. Syu, C. Cheng, T T.-H. Chang and H. Teng, *Adv. Funct. Mater*., 2010, **20**, 2255-2262.

28. N. Zhang, Y. Zhang and Y.-J. Xu, *Nanoscale*, 2012, **4**, 5792-5813.

29. N. Yang, Y. Liu, H. Wen, Z. Tang, H. Zhao, Y. Li and D. Wang, *ACS Nano,* 2013, **7**, 1504-1512.

30. G. Jiang, Z. Lin, C. Chen, L. Zhu, Q. Chang, N. Wang, W. Wei and H. Tang, *Carbon,* 2011, **49**, 2693-2701.

31. Y. Gao, X. Pu, D. Zhang, G. Ding, X. Shao and J. Ma, *Carbon,* 2012, **50**, 4093-4101.

32. H. Zhang, X. Lv, Y. Li, Y. Wang and J. Li, *ACS Nano,* 2009, **4**, 380-386.

33. X. Yin, H. Zhang, P. Xu, J. Han, J. Li, M. He**,** *RSC Adv.***,** 2013, **3**, 18474-18481.

34. Q. Xiang, J. Yu, M. Jaroniec, *Chem. Soc. Rev.***,** 2012,**41**, 782-796.

35. X. An, J. C. Yu, *RSC Adv.,* 2011, **1**, 1426-1434.

36. Q. Xiang, J. Yu, M. Jaroniec, *Nanoscale*, 2011, **3**, 3670-3678.

37. X. Zhou, T. Shi, J. Wua, H. Zhoua, *Appl. Surf. Sci.*, 2013, **287**, 359–368.

38. S. M.-Torres, L. M. P.-Martínez, J. L. Figueiredo, J. L. Faria, A. M.T. Silva, *Appl. Surf. Sci.* , 2013, **275**, 361–368.

39. C. Chen, W. Cai, M. Long, B. Zhou, Y. Wu, D. Wu and Y. Feng, *ACS Nano,* 2010, **4**, 6425-6432.

40. G. S. Anjusree, A. S. Nair, S. V. Nair and S. Vadukumpully, *RSC Advances,* 2013, **3**, 12933-12938.

41. S. D. Perera, R. G. Mariano, K. Vu, N. Nour, O. Seitz, Y. Chabal and K. J. Balkus, *ACS Catal.*, 2012, **2**, 949-956.

42. N. R. Khalid, E. Ahmed, Z. Hong, L. Sana and M. Ahmed, *Curr. Appl.Phys*., 2013, **13**, 659-663.

43. Q. Huang, S. Tian, D. Zeng, X. Wang, W. Song, Y. Li, W. Xiao and C. Xie, *ACS Catal*., 2013, **3**, 1477-1485.

44. L. Ci, L. Song, C. Jin, D. Jariwala, D. Wu, Y. Li, A. Srivastava, Z. F. Wang, K. Storr, L. Balicas, F. Liu and P. M. Ajayan, *Nat Mater.,* 2010, **9**, 430-435.

45. D. C. Marcano, D. V. Kosynkin, J. M. Berlin, A. Sinitskii, Z. Sun, A. Slesarev, L. B. Alemany, W. Lu and J. M. Tour, *ACS Nano*, 2010, **4**, 4806-4814.

46. D. Li, M.B. Muller, S. Gilje, R.B. Kaner and G.G.Wallace, *Nat Nano.,* 2008, **3,** 101-105.

47. P. Hohenberg and W. Kohn, *Phys. Rev*., 1964, **136**, 864-871.

48. W. Kohn and L. Sham, *Phys. Rev. A: At. Mol. Opt. Phys*., 1965, **140**, 1133-1138.

49. G. Kresse and J. Hafner, *Phys. Rev. B*, 1994, **49**, 1425114269.

50. G. Kresse and J. Furthmüller, *Comput. Mater. Sci*.,1996, **6**, 15-50.

51. J. P. Perdew, J. A. Chevary, S. H. Vosko, K. A. Jackson, M. R. Pederson, D. J. Singh and C. Fiolhais, *Phys. Rev. B,* 1992, **46**, 6671-6687.

52. J. P. Perdew and Y. Wang, *Phys. Rev. B*, 1992, **45**, 13244-13249.

53. T. Xu, L. Zhang, H. Cheng and Y. Zhu, *Appl. Catal. B: Environ*., 2011, **101**, 382-387.

54. T. Lu, R. Zhang, C. Hu, F. Chen, S. Duo and Q. Hu, *Phys. Chem. Chem. Phys.,* 2013, **15**, 12963-12970.

55. H.-Na Kim, H. Yoo and J. H. Moon, *Nanoscale*, 2013, **5**, 4200-4204.

56. N. K. Allam, F. Alamgir, & M. A. El-sayed, *ACS Nano*, 2010, **4**, 5819-5826.

57. X. H. Wang, J. G. Li, H. Kamiyama, Y. Moriyoshi and T. Ishigaki, *J. Phys. Chem. B,* 2006, **110**, 6804-6809.

58. W. Geng, H. Liu and X. Yao, *Phys. Chem. Chem.Phys*., 2013, **15**, 6025-6033.

59. Y. Liu, D.-P. Wang, Y.-X. Yu and W.-D. Zhang, *Int. J. Hydrogen Energy,* 2012, **37**, 9566-9575.

Graphical Abstract

Efficient visible light photodegradation of Methylene blue using TiO_2- graphene based composites has been reported. DFT calculations corroborate the mechanism for Ti-O-C bond formation, leading to an additional band edge and band gap tuning.